

Accepted Manuscript

Hydrothermal syntheses of tungsten doped TiO_2 and TiO_2/WO_3 composite using metal oxide precursors for charge storage applications

Bhupender Pal, Bincy Lathakumary Vijayan, Syam G. Krishnan, Midhun Harilal, Wan Jeffrey Basirun, Adrian Lowe, Mashitah M. Yusoff, Rajan Jose

PII: S0925-8388(18)30066-5

DOI: [10.1016/j.jallcom.2018.01.065](https://doi.org/10.1016/j.jallcom.2018.01.065)

Reference: JALCOM 44529

To appear in: *Journal of Alloys and Compounds*

Received Date: 2 August 2017

Revised Date: 29 December 2017

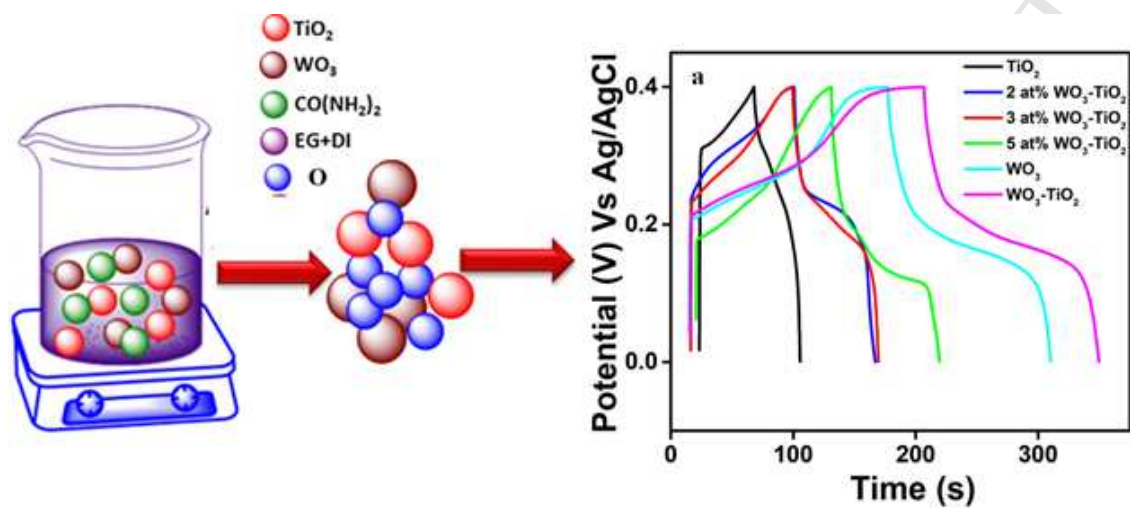
Accepted Date: 4 January 2018

Please cite this article as: B. Pal, B.L. Vijayan, S.G. Krishnan, M. Harilal, W.J. Basirun, A. Lowe, M.M. Yusoff, R. Jose, Hydrothermal syntheses of tungsten doped TiO_2 and TiO_2/WO_3 composite using metal oxide precursors for charge storage applications, *Journal of Alloys and Compounds* (2018), doi: 10.1016/j.jallcom.2018.01.065.

This is a PDF file of an unedited manuscript that has been accepted for publication. As a service to our customers we are providing this early version of the manuscript. The manuscript will undergo copyediting, typesetting, and review of the resulting proof before it is published in its final form. Please note that during the production process errors may be discovered which could affect the content, and all legal disclaimers that apply to the journal pertain.



Graphical abstract



Hydrothermal syntheses of tungsten doped TiO₂ and TiO₂/WO₃ composite using metal oxide precursors for charge storage applications

Bhupender Pal¹, Bincy Lathakumary Vijayan¹, Syam G. Krishnan¹, Midhun Harilal¹, Wan Jeffrey Basirun,² Adrian Lowe,³ Mashitah M. Yusoff,¹ Rajan Jose^{1*}

¹Nanostructured Renewable Energy Materials Laboratory, Faculty of Industrial Sciences and Technology, Universiti Malaysia Pahang, 26300 Kuantan, Malaysia; ²Department of Chemistry, Faculty of Science, University of Malaya, 50603, Malaysia; ³Research School of Engineering, Australian National University, Canberra 0200, Australia; *E-mail: rjose@ump.edu.my

Abstract

Synthesis of advanced functional materials through scalable processing routes using greener approaches is essential for process and product sustainability. In this article, syntheses of nanoparticles of titanium dioxide (TiO₂), tungsten trioxide (WO₃), WO₃-doped titanium dioxide (W-TiO₂) and TiO₂/WO₃ composite at hydrothermal conditions using corresponding metal oxide precursors are described. Electrochemical charge storage capabilities of the above materials are measured using cyclic voltammetry, charge-discharge cycling and electrochemical impedance spectroscopy in aqueous KOH electrolyte. The TiO₂ and the WO₃ nanoparticle showed a specific charge (Q) of ~12 and ~36 mA·h·g⁻¹ at a current density of 2 A·g⁻¹ in 6 M KOH, respectively. The Q of TiO₂ increased upon W doping up to 25 mA·h·g⁻¹ for 5 wt% W-TiO₂ and the WO₃/TiO₂ composite showed the highest storage capability (Q ~40 mA·h·g⁻¹). Changes in the charge storage capabilities of the doped and composite materials have been correlated to materials properties.

Keywords: Green synthesis; Nanocomposite; Renewable Energy; Battery type electrode; Supercapacitors.

1. Introduction

Titanium dioxide (TiO_2) and tungsten trioxide (WO_3) are important low cost functional materials due to their chemical stability, non-toxicity, semiconducting, electrochemical and optoelectronic properties [1-5]; consequently, with wide range of applications, such as sensors, lithium ion batteries, photocatalysis, catalyst supports, electrode for solar cells and electrochromic applications [6-8]. The TiO_2/WO_3 composite and W-doped TiO_2 have been investigated for many applications due to their promising properties, for example the TiO_2 supported WO_3 are very efficient heterogeneous catalyst for alkene isomerization and redox reactions [9]. Pan *et al.* [10] synthesized highly ordered cubic mesoporous WO_3/TiO_2 thin films and reported a higher photocatalytic activity compared to the pure TiO_2 film. Reyes-Gil *et al.* reported that the nanostructured composite of WO_3/TiO_2 showed higher ion storage capacity and better stability as compared to the pure WO_3 and TiO_2 nanostructures [11, 12]. The W-doped TiO_2 has shown higher electrical conductivity than TiO_2 and improved performance in dye sensitized solar cells [13].

There have been many reports on the energy storage properties of both TiO_2 and WO_3 as electrodes for lithium ion batteries [14, 15] and supercapacitors [16, 17]. Among various pseudo-supercapacitor materials, TiO_2 has received exceptional interest because of their low cost, excellent chemical stability, abundance and low environmental impact [18]. However, the semiconducting nature and poor electrical conductivity of TiO_2 attributes to the lower electrochemical activity thereby reducing its specific capacitance ($< 50 \text{ F g}^{-1}$) [19]. Many efforts have been focused to overcome these issues such as developing TiO_2 architectures (nanotube arrays) with sufficient open structures thereby providing a direct pathway for charge transport to

overcome the low ion diffusion coefficient [20]; improving the electrical properties of TiO₂ by metallic and nonmetallic doping [13]. The doping of TiO₂ with non-metals (N and H) and transition metals (Ni³⁺, Zr⁴⁺, W⁶⁺, Ce⁴⁺, V⁵⁺, Nb⁵⁺, Fe³⁺) is considered an efficient method to improve the electrical conductivity of TiO₂ [21-23]. Recently, a significant improvement in the capacitive performance was realized through the hydrogenation of one-dimensional anodic TiO₂ nanotube arrays due to the improved electrochemical activity and electrode conductivity with hydrogen induced Ti³⁺ sites in the TiO₂ lattices [24]. However, the scalability of these one-dimensional anodic TiO₂ nanotube arrays through anodization is rather poor. The fabrication of TiO₂/carbon hybrid is another way to improve the capacitance of TiO₂ due to the improved conductivity and high specific surface area of carbon materials [25, 26]. Although the electrochemical performances of these composites are improved by combining the merits of both components and improving the limitations of each component, these composites still suffer from low capacitances in the range of 100-200 Fg⁻¹ and poor rate capability under various aqueous and non-aqueous electrolytes. Therefore, to further extend the charge storage and rate capability of TiO₂-based supercapacitors, cost effective and scalable approaches are highly desirable.

On the other hand, WO₃ possesses desirable properties such as multiple oxidation states and resistance to strong acids for supercapacitor applications [27]. The utilization of crystalline WO₃ mixtures as electrodes resulted in a capacitance of up to 290 F·g⁻¹ as reported by Chang *et al* [28]. Jeong *et al.* fabricated WO₃ nanoparticle impregnated ZrO₂-SiO₂ sheets for energy storage and reported a capacitance of 313 F·g⁻¹ [29]. Hercule *et al.* reported that the hierarchical architecture allows for the synergistic contribution of mixed electrode materials and leads to a better electrochemical performance [30]. As mentioned above, there are reports of doping WO₃

with TiO_2 for enhanced electrical conductivity and also the preparation of $\text{TiO}_2\text{-WO}_3$ composite for biosensor application [31].

The above doped materials and composites have been prepared using wet-chemical techniques using soluble precursors, such as hydrolytic sol-gel, hydrothermal/solvothermal, and electrochemical deposition with notable enhancements in the targeted properties [32-35]. While atomic scale mixing can be achieved using these techniques, they are still time-consuming, complicated and involves multistep processes. Besides, most of the soluble precursors are highly reactive, pyrophoric, corrosive and offer significant challenges before scaling up for materials production. On the other hand, metal oxide precursors are stable and non-corrosive; however, atomic level mixing cannot be achieved using them and the resulting materials obtained through solid state reaction are coarse grained with inferior properties. In this paper, we report the use of metal oxide precursors in a hydrothermal reaction to produce fine powders of W-doped TiO_2 (W-TiO_2) and WO_3/TiO_2 composite with superior energy storage properties than their undoped and binary counterparts. The green synthetic method and promising energy storage capabilities thereby could make this approach to be industrially viable. Although earlier studies considered TiO_2 and WO_3 as pseudocapacitor materials and reported the charge storability in terms of Fg^{-1} , the occurrence of redox peaks in the cyclic voltammograms and nonlinear discharge behavior during galvanostatic measurements classify them as battery-type electrode materials [36]. Therefore, the storage parameter evaluated in this work is expressed in units of mAhg^{-1} .

2. Experimental Details

2.1. Materials

All the chemicals used in the present work were of analytical reagent (AR) grade. The urea [$\text{CO}(\text{NH}_2)_2$], ethylene glycol [$(\text{CH}_2\text{OH})_2$], potassium hydroxide [KOH], polyvinylidene

fluoride [$-(C_2H_2F_2)_n-$], N-methyl-2-pyrrolidinone [C_5H_9NO], hydrochloric acid [HCl], titanium dioxide [TiO_2], and tungsten trioxide [WO_3] were obtained from Sigma-Aldrich and used as received. De-ionized water was used for the entire synthesis and application purposes.

2.2. Synthesis and Characterization of W-doped TiO_2 and TiO_2/WO_3 composite

In a typical synthesis, 60 mM of $CO(NH_2)_2$ and 8 mM of TiO_2 were dissolved in 80 ml of $(CH_2OH)_2$ and 40 ml de-ionized water. The solution was mixed well by stirring for two hours. Then, the resultant solution was transferred into a Teflon lined stainless steel autoclave, sealed, and heated in an oven at 150 °C for 5 h 30 min. The final product was washed with de-ionized water, dried at 60 °C for 12 h and calcined at 460 °C for 3 h. The WO_3 nanoparticles were prepared with same procedures as the TiO_2 . The 2, 3 and 5 wt% of W-doped TiO_2 were prepared with the same procedures except changing the concentration of WO_3 for the respective weight percentage. For the synthesis of WO_3/TiO_2 nanocomposite, 4 mM of WO_3 , 4 mM of TiO_2 and 60 mM of $CO(NH_2)_2$ were dissolved in 80 ml of $(CH_2OH)_2$ and 40 ml de-ionized water. The solution was mixed well by stirring for two hours. Then, the resultant solution was transferred into a Teflon lined stainless steel autoclave, sealed, and heated in an oven at 150 °C for 5 h 30 min. The final product was washed with de-ionized water, dried at 60 °C for 12 h and calcined at 460 °C for 3 h. The schematic presentation for the materials preparation is also shown in scheme 1. The crystal structures of all materials were characterized by powder X-ray diffraction (XRD) using a Rigaku Miniflex II X-ray diffractometer employing Cu $K\alpha$ radiation ($\lambda = 1.5406 \text{ \AA}$). The morphology and microstructure of these materials were characterized by field emission scanning electron microscopy (7800F, FE-SEM, JEOL, USA). Raman spectroscopy was performed using a Raman spectrometer (Horiba Jobin Yvon HR 8000, UK). The BET (Brunauer-Emmett-Teller)

surface area of all materials was measured by Micromeritics, Tristar 3000, USA. The FTIR studies were performed using a FTIR spectrometer (Thermo Scientific Nicolet iS50).

2.3. Electrode fabrication for electrochemical studies

The supercapacitor electrodes were fabricated on pre-cleaned nickel foam substrates. The nickel foam was cleaned by degreasing in acetone, etching in 1 M HCl for 15 minutes and subsequently washing in water and ethanol for 5 min each. The working electrode was prepared by mixing the as prepared samples with polyvinylidene fluoride (PVDF) and carbon black (Super P conductive, Alfa Aesar) in 80:10:10 ratios. A set of electrodes containing a 1:1 mixture of WO_3 and TiO_2 powders, which were physically mixed, were also prepared to evaluate the relative advantage of the hydrothermal reaction. The above mixture was stirred in N-methyl-2-pyrrolidinone for better homogeneity. The as-prepared slurry was then pasted onto the nickel foam substrate (area $\sim 1 \text{ cm}^2$) and dried in an oven at $60 \text{ }^\circ\text{C}$ for 24 h. The mass-loading of the active material was $\sim 2.5 \text{ mg cm}^{-2}$. The dried electrode was then pressed using a pelletizer at a pressure of 5 ton. The electrochemical properties of the devices were studied by cyclic voltammetry (CV), galvanostatic charge-discharge cycling (GCD) and electrochemical impedance spectroscopy (EIS) in KOH electrolyte. The electrochemical properties in a three-electrode configuration were obtained at room temperature using a potentiostat–galvanostat (PGSTAT M101, Metrohm Autolab B.V., The Netherlands) employing NOVA 1.9 software. A platinum rod and a saturated Ag/AgCl electrode were used as the counter and reference electrodes, respectively.

3. Results and Discussions

3.1. Structural and morphological characterization of the as prepared samples

The structural characterization of the as prepared samples was performed by power x-ray diffraction (XRD) technique. The XRD patterns of TiO₂, (2, 3 and 5 wt%) W-TiO₂, WO₃ and WO₃/TiO₂ nanocomposite (1:1) are shown in Fig. 1 (a and b). The XRD pattern reveals that TiO₂ is present in the anatase form in all samples. For the bare TiO₂, peaks at 2θ (25.5°, 37.7° and 48.5°) are well matched with the anatase phase, JCPDS 02-0406 [37]. The various weight percentages (2, 3 and 5 wt%) of WO₃ on TiO₂ show a small shift in the characteristic peaks of TiO₂ as given in Fig. 1(b) which might be due to the difference in the ionic radii between W⁶⁺ (0.60 Å) and Ti⁴⁺ (0.605 Å) for the six-fold coordination [13] thereby inducing some changes in the lattice parameters. The lattice parameters of these samples were calculated using the procedures described elsewhere [38] from the XRD patterns, and are summarized in Table 1. The XRD patterns of WO₃ shown in Fig. 1(a) are well indexed with the monoclinic crystal structure of WO₃ (JCPDS file No. 43-1035) and strong diffraction peaks indicate the good crystallinity of the material [39]. In the XRD patterns (Fig. 1a) of WO₃/TiO₂ (1:1) nanocomposites, all peaks are well indexed to both TiO₂ anatase and WO₃ monoclinic crystal structure, due to equimolar ratio of TiO₂ and WO₃ [33].

After the structural identification, field emission scanning electron microscopy (FE-SEM) was performed to investigate the morphology and topography of the as prepared samples. Fig. 2 (a) shows the FE-SEM images of the as prepared TiO₂ nanoparticles; all the particles are uniform and spherical in shape with a diameter ~30 nm. After the incorporation of WO₃ in TiO₂, there is only small aggregation in the particles as shown in Fig. 2 (b-d), but the aggregation increases with the concentration of tungsten as clearly seen in these images. Fig. 2 (e) shows the FE-SEM image of pure WO₃ nanoparticles, where the particles are spherical in shape with a diameter range between 60-80 nm. When an equimolar ratio (1:1) of WO₃ and TiO₂ were mixed for the

preparation of WO_3/TiO_2 nanocomposite, the particle size increases with diameter between 70-100 nm as shown in Fig. 2 (f). The particles are aggregated with very small uniformity in their sizes.

Figure 3 (a and b) shows the Raman spectra of TiO_2 , W-TiO_2 (2, 3 and 5 wt%), WO_3 and WO_3/TiO_2 nanocomposite. The Raman spectra of the pure TiO_2 showed (Fig. 3a) peaks at 141, 397, 516 and 639 cm^{-1} and agree with the results of Ohsaka *et al.* [40]. In case of 2, 3 and 5 wt% of W-TiO_2 , the band position was slightly shifted as shown in the inset of Fig. 3a. The high intensity peak at 141 cm^{-1} is consistent with the Ti-Ti covalent interactions (2.96 Å; 0.29 valence units) [41]. The Ti-O bands at 516 and 639 cm^{-1} yield the calculated Ti-O bond lengths of 1.98 and 1.90 Å while the O-O interactions occurs at 397 cm^{-1} [42]. For the pure WO_3 , the main bands at 805 and 714 cm^{-1} are attributed to the stretching of O-W-O modes while the lower wavenumber region between 132-326 cm^{-1} are attributed to the O-W-O deformation lattice modes as shown in Fig. 3 (b), in close agreement with the results of Daniel *et al.* [43]. A Raman spectrum of the WO_3/TiO_2 nanocomposite is shown in the inset of Fig 3b, where there are two sharp peaks at 141 and 886 cm^{-1} region. The peak at 141 cm^{-1} is assigned to the Ti-Ti covalent interactions while 886 cm^{-1} is assigned to the $\text{W}^{6+}=\text{O}$ interaction, because the chemical bonds with W^{6+} are stronger than those with the W^{5+} and W^{4+} , therefore the Raman peaks for $\text{W}^{6+}-\text{O}$ and $\text{W}^{6+}=\text{O}$ appear at higher wavenumbers (i.e. higher energies) [44]. The peak at 691 cm^{-1} is assigned to the O-W-O stretching. The peaks between 397 and 637 cm^{-1} are assigned to the Ti-O and O-O interactions [42]. Therefore, the Raman spectra and XRD patterns show clear confirmation of the WO_3/TiO_2 nanocomposites. The nitrogen adsorption-desorption isotherms were measured to determine the specific surface area of all the samples (Fig. S1). The isotherm displays a typical type IV curve with a hysteresis loop at a relative pressure (P/P_0) between 0.0

and 1.0, suggesting that the pure TiO₂ is more mesoporous compared to the other samples [45]. The BET surface area of the pure TiO₂, 2, 3 and 5 wt% W-TiO₂, WO₃ and WO₃/TiO₂ nanocomposite was 299.9821 m²/g, 51.1094 m²/g, 50.3819 m²/g, 48.7358 m²/g, 12.1750 m²/g, 44.3539 m²/g, respectively, which validates the FE-SEM and XRD results.

3.2. Electrochemical properties of the as prepared samples

3.2.1. Galvanostatic charge–discharge (GCD) studies

The performance of the fabricated electrode as a supercapacitor is determined by GCD cycling in 6 M KOH. Fig. 4a shows the comparison of the GCD curves of all the electrodes at 1 A·g⁻¹. The asymmetries in the CD curve denote that all the electrodes follow a battery type charge storage behavior [36]. Furthermore, the composite electrode shows an improved charge-discharge properties compared to the other electrodes. The charge stored (Q) in the electrodes can be determined from the equation :

$$Q = \frac{I \times t}{m} \quad (1)$$

where I , t and m have their usual meaning as mentioned in our previous publication [46]. The charge storage can be calculated by determining the discharge rate of the electrodes. The discharge curves of all the electrodes are shown in Fig. S4 (supplementary information). One could observe that the discharge rate increases with the increase in the current density, thereby reducing the charge stored at higher current densities. The variation of charge with current density of all electrodes is compiled in Fig. 4(b). This decrease can be attributed to the surface charge polarization of the electrode at higher current densities [19]. The WO₃/TiO₂ nanocomposite electrode demonstrated superior charge storage of ~40 mA·h·g⁻¹ compared to the

pure WO_3 ($\sim 36 \text{ mA}\cdot\text{h}\cdot\text{g}^{-1}$) and TiO_2 ($\sim 12 \text{ mA}\cdot\text{h}\cdot\text{g}^{-1}$) at $1 \text{ A}\cdot\text{g}^{-1}$. Interestingly, the physically mixed electrode showed the lowest capacitance among all the electrodes studied here ($\sim 2.6 \text{ mA h g}^{-1}$) at 1 A g^{-1} (Supplementary Information, Fig. S5), thereby validating the effect of hydrothermal reaction on the charge storage characteristics of the materials reported herewith.

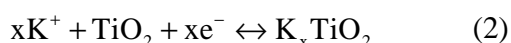
The charge storage of TiO_2 has improved with 2 wt% WO_3 ($\sim 18 \text{ mA}\cdot\text{h}\cdot\text{g}^{-1}$), 3 wt% WO_3 ($\sim 19 \text{ mA}\cdot\text{h}\cdot\text{g}^{-1}$) and 5 wt% WO_3 ($\sim 25 \text{ mA}\cdot\text{h}\cdot\text{g}^{-1}$). The addition of WO_3 decreased the potential drop (IR drop) of TiO_2 from 3.8 mV to 3.4, 3.2, and 3 mV, for 2 wt%, 3 wt% and 5 wt% W- TiO_2 respectively. The IR drop for the pure WO_3 and WO_3/TiO_2 nanocomposite was 2.8 mV and 2 mV, respectively. The decrease in the IR drop of the electrodes with WO_3 modification suggests that the internal resistance of the electrode material (ESR) also decreases with the increase in the weight percentage of WO_3 in TiO_2 . The ESR of the electrodes can be determined by the ratio of the potential drop to the change in the current. The internal resistance of the electrodes was $3.2 \Omega \text{ cm}^{-2}$, $2.8 \Omega \text{ cm}^{-2}$, $2.4 \Omega \text{ cm}^{-2}$, and $2.2 \Omega \text{ cm}^{-2}$, for TiO_2 , 2 wt% W- TiO_2 , 3 wt% W- TiO_2 and 5 wt% W- TiO_2 , respectively. The internal resistance of the WO_3 and WO_3/TiO_2 nanocomposite electrode was $1.6 \Omega \text{ cm}^{-2}$ and $1.3 \Omega \text{ cm}^{-2}$, respectively. Therefore, it is confirmed that an increase in the conductivity, hence the charge storage in TiO_2 was due to the tungsten addition.

The stability of the electrodes was analyzed by continuous charge-discharge cycling for 3000 cycles at $5 \text{ A}\cdot\text{g}^{-1}$. Fig. 5 compares the stability curves of all the electrodes. The pure TiO_2 electrode shows 100 % capacity retention ($\sim 8 \text{ mA}\cdot\text{h}\cdot\text{g}^{-1}$) for the first 250 cycles. Later the capacitance decreases by 5 % at the end of 500 cycles. The capacity decreases to 70 % of its initial capacitance ($\sim 5.6 \text{ mA}\cdot\text{h}\cdot\text{g}^{-1}$) at the end of the 3000 cycles. Similarly, the capacity of WO_3 faded to 80 % of its initial value ($\sim 12 \text{ mA}\cdot\text{h}\cdot\text{g}^{-1}$) after 3000 cycles. It can be observed that the

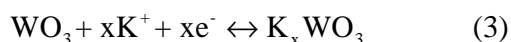
capacity retention of TiO₂ improved to 72 % (~6 mA·h·g⁻¹), 75 % (~6.8 mA·h·g⁻¹) and 77 % (~9 mA·h·g⁻¹) after 3000 cycles, for the 2 wt%, 3 wt% and 5 wt% W-TiO₂ modification, respectively. The WO₃/TiO₂ capacity retention was 100% up to 1000 cycles (~19 mA·h·g⁻¹) before fading at 92% of retention (~17.5 mA·h·g⁻¹), at the end of the 3000 cycles. This improvement in capacity retention also justifies the advantage of the composite electrode. The dissolution of the electrode material in the KOH electrolyte during long term cycling could have attributed to its lower cycling stability [46].

3.2.2. Cyclic voltammetry studies

The cyclic voltammetry measurements were performed to evaluate the electrochemical behavior of the electrodes between 0-0.4 V in 6 M KOH. Fig. 6(a) shows the CV curves of TiO₂, (2, 3 and 5 wt%) W-TiO₂, WO₃ and WO₃/TiO₂ nanocomposite measured at a scan rate of 2mVs⁻¹ in 6 M KOH aqueous electrolyte. This lower scan rate indicates an efficient diffusion of hydroxyl ions into the electrode, thereby clearly revealing the electrochemical processes. The CV curves of all electrodes at various scan rates are given in the supplementary information, S3. It can be observed that all the CV curves consist of well-defined redox peaks whose position is shifted from lower to higher scan rate. This shift is due to the charge polarization in the electrode from lower to higher scan rate [47]. Furthermore, the redox peak in the CV curve indicates a battery type charge storage behavior for all the electrodes [36]. The redox peaks in the Ti electrodes can be attributed to the insertion/de-insertion of the K⁺ ions in/out of the oxides with concomitant reduction/oxidation of the Ti ions [48], which can be expressed as



For the WO_3 electrodes, the redox peaks obtained can be attributed to the intercalation/de-intercalation of x number of positive ions with an equal number of electrons (e^-) [49] as depicted in the following equation



where the factor ‘ x ’ in both equations can vary from 0 to 1. The WO_3 - TiO_2 electrode combines both the processes mentioned in equation 1 and 2 during the charge storage processes. The high charging plateau for the WO_3 and WO_3/TiO_2 composite also suggests the combination of redox reaction mentioned in equation (2) and (3). A high voltammetric current (2.1 mA) is generated from the WO_3/TiO_2 nanocomposite compared to <1 mA of the pure TiO_2 at 2 mV s^{-1} scan rate. This effect could be attributed to the enhanced faradic reaction due to the improved electrical conductivity and synergetic effect of the WO_3/TiO_2 nanocomposite.

The improved current response of WO_3/TiO_2 nanocomposite generates an improved specific charge capacity (Q); where Q could be evaluated from CV curves using the following equation:

$$Q = \int_{E_1}^{E_2} \frac{i(E) dE}{2 \nu m} \quad (3)$$

where ‘ m ’ is the mass of the active material, ‘ ν ’ is the scan rate, $E_2 - E_1$ is the potential window and ‘ i ’ is the current at each potential [50]. The term ‘2’ in the equation 2 signifies the involvement of both cathodic and anodic area. The Q value obtained for the composite electrode ($\sim 41 \text{ mA h}^{-1}$) is superior to the individual WO_3 ($\sim 38 \text{ mA h g}^{-1}$) and TiO_2 ($\sim 15 \text{ mA h g}^{-1}$). Fig. 6(b) shows the variation of Q with scan rate of all electrode materials. One could observe that the ‘ Q ’ increases with the increasing percentage of WO_3 ; the Q achieved at 2 mV s^{-1} was ~ 19 , ~ 21 ,

and $\sim 27 \text{ mA h g}^{-1}$ for 2wt%, 3wt% and 5wt% W-TiO₂, respectively. Similar to the GCD studies, the surface charge polarization of all electrodes decreases the Q with the increase in scan rate. In addition, the reason for the improved performance of the electrodes is due to the WO₃ addition, which can be analyzed by electrochemical impedance spectroscopy studies in the next section.

3.2.3. Electrochemical impedance spectroscopy studies

The characteristic electrode resistances such as electrode series resistance (R_S), charge transfer resistance (R_{CT}) and the capacitive behavior of the electrodes can be determined from EIS measurements. Fig. 7 shows the Nyquist plot obtained from the EIS measurements between 1mHz – 10 KHz. One could observe that the Nyquist plot consists of a (i) low frequency region (<5 Hz) (ii) intermediate frequency region (<1 kHz) and (iii) high frequency region (>1 kHz) [51]. The inset of Fig.7 represents the high frequency region which consists of a semicircle whose diameter represents the charge transfer resistance R_{CT} . In addition the high frequency inset also represents the electrode series resistance (R_S). The intermediate frequency region represents the capacitive effects while the lower frequency region represents the Warburg impedance. From the high frequency inset, one could observe that the R_S value of WO₃/TiO₂ composite electrode is lower ($\sim 0.64 \Omega$) compared to WO₃ ($\sim 0.71 \Omega$), 5wt% W-TiO₂ (0.75Ω), 3wt% W-TiO₂ (0.82Ω), 2wt% W-TiO₂ (0.82Ω) and TiO₂ (0.93Ω). Therefore a considerable reduction in the resistance of the TiO₂ electrode with the formation of WO₃-TiO₂ could be observed. Furthermore, the resistance of TiO₂ electrode decreased with the increase of WO₃ due to the enhanced conductivity of the electrode. Since the R_S combines the electrolyte and electrode resistances, as well as the contact resistance between electrode and electrolyte, the WO₃/TiO₂ electrode offers improved solvated ion transfer from the electrolyte to electrode, thereby increasing the charge storage. The kinetic resistance at the electrode/electrolyte interface is determined by R_{CT} value of

the electrode. The R_{CT} determined from the Nyquist plot of the WO_3/TiO_2 electrode was lower (0.26Ω) compared to 0.34Ω , 0.42Ω , 0.5Ω , 0.62Ω and 0.72Ω for WO_3 , 5 wt%, 3 wt%, 2 wt% W- TiO_2 and pure TiO_2 electrodes, respectively. The ESR determined from EIS for all the electrodes is lower compared to ESR value from GCD studies, thereby validating earlier reports [52]. Therefore, the combination of enhanced charge transfer and electrode conductivity improved the ion intercalation to the pores of the electrode materials thereby improving the charge storage in the composite electrode.

4. Conclusions

In conclusion, we have shown that WO_3/TiO_2 nanocomposite have higher specific capacitance than the bare TiO_2 , WO_3 and lower weight percentage (2, 3 and 5 wt%) of WO_3 in TiO_2 which could be attributed to its improved electrical conductivity and synergetic effect of the composite. Cyclic voltammetric measurements show that the superior electrical conductivity of WO_3/TiO_2 nanocomposite enhances the electrode to achieve higher ion diffusivity compared to the other electrodes in this study. The WO_3/TiO_2 electrode demonstrated a superior charge storage of $\sim 39 \text{ mA}\cdot\text{h}\cdot\text{g}^{-1}$ with lower electrode resistance (0.64Ω), charge transfer resistance (0.26Ω) and improved cyclic stability of $\sim 92\%$ after 3000 cycles. The low cost, high chemical stability, non-toxicity and high abundance of TiO_2 in the earth's crust and promising results achieved herewith offer unique opportunities to develop practical energy storage devices.

Acknowledgements

Bhupender Pal acknowledges the Research & Innovation Department of Universiti Malaysia Pahang (<http://ump.edu.my>) for award of Postdoctoral Fellowship. This project is funded under Flagship Strategic Leap 3 of Universiti Malaysia Pahang (RDU 172201).

References

- [1] F.F. Chen, F.L. Cao, H.X. Li, Z.F. Bian, Exploring the important role of nanocrystals orientation in TiO₂ superstructure on photocatalytic performances, *Langmuir* 31 (2015) 3494.
- [2] J. Wang, Z.Q. Lin, Dye-Sensitized TiO₂ Nanotube solar cells with markedly enhanced performance via rational surface engineering. *Chem. Mater.* 22 (2010) 579.
- [3] Z. Chen, J. Zhao, X. Yang, Q. Ye, K. Huang, C. Hou, Z. Zhao, J. You, Y. Li, Fabrication of TiO₂/WO₃ composite nanofibers by electrospinning and photocatalytic performance of the resultant fabrics, *Ind. Eng. Chem. Res.* 55 (2016) 80-85.
- [4] C. Santato, M. Odziemkowski, M. Ulmann, J. Augustynski, Crystallographically oriented mesoporous WO₃ films: synthesis, characterization, and applications, *J. Am. Chem. Soc.* 123 (43), (2001) 10639-10649.
- [5] C. Wanga, X. Zhang, B. Yuan, Y. Wang, P. Sun, D. Wanga, Y. Wei, Y. Liu, Multi-heterojunction photocatalysts based on WO₃ nanorods: Structural design and optimization for enhanced photocatalytic activity under visible light, *Chem. Eng. J.* 237 (2014) 29-37.
- [6] K. Park, K. Min, Y. Jin, S. Seo, G. Lee, H. Shim, D. Kim, Enhancement of cyclability of urchin-like rutile TiO₂ submicron spheres by nanopainting with carbon, *J. Mater. Chem.* 22 (2012) 15981-15986.
- [7] F. Huang, Z. Fu, A. Yan, W. Wang, H. Wang, Y. Wang, J. Zhang, Y. Cheng, Q. Zhang, Facile synthesis, growth mechanism, and UV-Vis spectroscopy of novel urchin-like TiO₂/TiB₂ heterostructures, 9 (2009) 4017-4022.
- [8] X. Chen, L. Liu, P.Y. Yu, S.S. Mao, Increasing solar absorption for photocatalysis with black hydrogenated titanium dioxide nanocrystals, *Science* 331 (2011) 746-750.
- [9] X.F. Yu, N.Z. Wu, H.Z. Huang, Y.C. Xie, Y.Q. Tang, A study on the monolayer dispersion of tungsten oxide on anatase, *J. Mater. Chem.* 11 (2001) 3337-3342.
- [10] J.H. Pan, W.I. Lee, Preparation of highly ordered cubic mesoporous WO₃/TiO₂ films and their photocatalytic properties, *Chem. Mater.* 18 (2006) 847.

- [11] K.R. Reyes-Gil, D.B. Robinson, WO₃-enhanced TiO₂ nanotube photoanodes for solar water splitting with simultaneous wastewater treatment, *ACS Appl. Mater. Interfaces* 5 (2013) 12400.
- [12] K.R. Reyes-Gil, Z.D. Stephens, V. Stavila, D.B. Robinson, Composite WO₃/TiO₂ nanostructures for high electrochromic activity, *ACS Appl. Mater. Interfaces* 7 (2015) 2202.
- [13] P.S. Archana, A. Gupta, M.M. Yusoff, R. Jose, Tungsten doped titanium dioxide nanowires for high efficiency dye-sensitized solar cells, *Phys. Chem. Chem. Phys.* 16 (2014) 7448-7454.
- [14] Y.Q. Wang, L. Gu, Y.G. Guo, H. Li, X.Q. He, S. Tsukimoto, Y. Ikuhara L.J. Wan, Rutile-TiO₂ nanocoating for a high-rate Li₄Ti₅O₁₂ anode of a lithium-ion battery, *J. Am. Chem. Soc.*, 134 (2012) 7874-7879.
- [15] K. Huang, Q. Pan, F. Yang, S. Ni, X. Wei, D. He, Controllable synthesis of hexagonal WO₃ nanostructures and their application in lithium batteries, *J. Phys. D: Appl. Phys.* 41 (2008) 155417.
- [16] X. Lu, G. Wang, T. Zhai, M. Yu, J. Gan, Y. Tong, Y. Li, Hydrogenated TiO₂ nanotube arrays for supercapacitors, *Nano. Lett.* 12 (2012) 1690-1696.
- [17] H. Zhou, X. Zou, K. Zhang, P. Sun, M. S. Islam, J. Gong, Y. Zhang, J. Yang, Molybdenum-tungsten mixed oxide deposited into titanium dioxide nanotube arrays for ultrahigh rate supercapacitors, *ACS Appl. Mater. Interfaces* 9 (22) (2017) 18699-18709.
- [18] B. Vidyadharan, P.S. Archana, J. Ismail, M.M. Yusoff, R. Jose, Improved supercapacitive charge storage in electrospun niobium doped titania nanowires, *RSC Adv.* 5 (2015) 50087-50097.
- [19] S.G. Krishnan, P.S. Archana, B. Vidyadharan, I.I. Misnon, B.L. Vijayan, V.M. Nair, A. Gupta, R. Jose, Modification of capacitive charge storage of TiO₂ with nickel doping, *J. Alloys Compd.* 684 (2016) 328-334.
- [20] H. Fan, H. Zhang, X. Luo, M. Liao, X. Zhu, J. Ma, Y. Song, Hydrothermal solid-gas route to TiO₂ nanoparticles/nanotube arrays for high-performance supercapacitors, *J. Power Sources*, 357 (2017) 230-240.

- [21] J. Song, X. Wang, J. Yan, J. Yu, G. Sun, B. Ding, Soft Zr-doped TiO₂ nanofibrous membranes with enhanced photocatalytic activity for water purification, *Sci. Rep.* 7 (2017) 1636.
- [22] S. Yao, S. Wang, S. Sun, Z. Shi, Preparation, characterization of Fe, Ce Co-doped flower-like TiO₂ photocatalysts and their properties in photocatalytic oxidation of arsenite, *Russ. J. Phys. Chem. A* 91 (2017) 1132-1137.
- [23] M. Asgharinezhad, A. Eshaghi, A. Arab, Fabrication and characterization of optical and electrical properties of vanadium doped titanium dioxide nanostructured thin film, *Inter. J. Light and Electron Optics*, 127 (2016) 8130-8134.
- [24] X. Lu, G. Wang, T. Zhai, M. Yu, J. Gan, Y. Tong, Y. Li, Hydrogenated TiO₂ nanotube arrays for supercapacitors, *Nano. Lett.* 12 (2012) 1690-1696.
- [25] J. Wang, W. Li, Y. Ge, J. Shen, Y. Zhao, Y. Zhang, J. Yuan, Design and synthesis of porous TiO₂@C nanotube bundles with enhanced supercapacitive performance, *Ceram. Int.* 43 (2017) 2876-2880.
- [26] Y. Liu, T. Gao, H. Xiao, W. Guo, B. Sun, M. Pei, G. Zhou, One-pot synthesis of rice-like TiO₂/graphene hydrogels as advanced electrodes for supercapacitors and the resulting aerogels as high-efficiency dye adsorbents, *Electrochim. Acta* 229 (2017) 239-252.
- [27] S. Yoon, E. Kang, J.K. Kim, C.W. Lee, J. Lee, Development of high-performance supercapacitor electrodes using novel ordered mesoporous tungsten oxide materials with high electrical conductivity, *Chem. Commun.*, 47 (2011) 1021-1023.
- [28] K.-H. Chang, C.-C. Hu, C.-M. Huang, Y.-L. Liu, C.-I. Chang, Microwave-assisted hydrothermal synthesis of crystalline WO₃-WO₃·0.5H₂O mixtures for pseudocapacitors of the asymmetric type, *J. Power Sources*, 196 (2011) 2387-2392.
- [29] G.H. Jeong, H.-M. Lee, J.-g. Kang, H. Lee, C.-K. Kim, J.-H. Lee, J.-H. Kim, S.-W. Kim, ZrO₂-SiO₂ nanosheets with ultrasmall wo₃ nanoparticles and their enhanced pseudocapacitance and stability, *ACS Appl. Mater. Inter.*, 6 (2014) 20171-20178.

- [30] K.M. Hercule, Q. Wei, A.M. Khan, Y. Zhao, X. Tian, L. Mai, Synergistic effect of hierarchical nanostructured $\text{MoO}_2/\text{Co}(\text{OH})_2$ with largely enhanced pseudocapacitor cyclability, *Nano Lett.*, 13 (2013) 5685-5691.
- [31] Y. Zhu, X. Su, C. Yang, X. Gao, F. Xiao, J. Wang, Synthesis of $\text{TiO}_2\text{-WO}_3$ nanocomposites as highly sensitive benzene sensors and high efficiency adsorbents, *J. Mater. Chem.*, 22 (2012) 13914-13917.
- [32] X. Chen, S.S. Mao, Titanium dioxide nanomaterials: synthesis, properties, modifications, and applications, *Chem. Rev.*, 107 (2007) 2891-2959.
- [33] V. Puddu, R. Mokaya, G. Li Puma, Novel one step hydrothermal synthesis of TiO_2/WO_3 nanocomposites with enhanced photocatalytic activity, *Chem. Commun. (Camb)*, (2007) 4749-4751.
- [34] D. Ke, H. Liu, T. Peng, X. Liu, K. Dai, Preparation and photocatalytic activity of WO_3/TiO_2 nanocomposite particles, *Mater. Lett.*, 62 (2008) 447-450.
- [35] K.K. Akurati, A. Vital, J.-P. Dellemann, K. Michalow, T. Graule, D. Ferri, A. Baiker, Flame-made WO_3/TiO_2 nanoparticles: Relation between surface acidity, structure and photocatalytic activity, *Appl. Catal. B: Environ.*, 79 (2008) 53-62.
- [36] T. Brousse, D. Bélanger, J.W. Long, To be or not to be pseudocapacitive?, *J. Electrochem. Soc.*, 162 (2015) A5185-A5189.
- [37] K. Sakurai, M. Mizusawa, X-ray diffraction imaging of anatase and rutile, *Anal. Chem.*, 82 (2010) 3519-3522.
- [38] P. S. Archana, R. Jose, T. M. Jin, C. Vijila, M. M. Yusoff and S. Ramakrishna, Structural and Electrical Properties of Nb-Doped Anatase TiO_2 Nanowires by Electrospinning, *J. Am. Ceram. Soc.*, 2010, 93, 4096-4102.
- [39] J. Zhang, S.A. Wessel, K. Colbow, Spray pyrolysis electrochromic WO_3 films: Electrical and X-ray diffraction measurements, *Thin Solid Films*, 185 (1990) 265-277.

- [40] T. Ohsaka, F. Izumi, Y. Fujiki, Raman spectrum of anatase, TiO_2 , *J. Raman Spectrosc.*, 7 (1978) 321-324.
- [41] H.C. Choi, Y.M. Jung, S.B. Kim, Size effects in the Raman spectra of TiO_2 nanoparticles, *Vib. Spectrosc.*, 37 (2005) 33-38.
- [42] J.C. Parker, R.W. Siegel, Calibration of the Raman spectrum to the oxygen stoichiometry of nanophase TiO_2 , *Appl. Phys. Lett.*, 57 (1990) 943-945.
- [43] M.F. Daniel, B. Desbat, J.C. Lassegues, B. Gerand, M. Figlarz, Infrared and Raman study of WO_3 tungsten trioxides and $\text{WO}_3 \cdot x\text{H}_2\text{O}$ tungsten trioxide hydrates, *J. Solid State Chem.*, 67 (1987) 235-247.
- [44] I.M. Szilágyi, J. Madarász, G. Pokol, P. Király, G. Tárkányi, S. Saukko, J. Mizsei, A.L. Tóth, A. Szabó, K. Varga-Josepovits, Stability and controlled composition of hexagonal WO_3 , *Chem. Mater.*, 20 (2008) 4116-4125.
- [45] S.M.F. Shaikh, S.S. Kalanur, R.S. Manea, O.-S. Joo, Monoclinic WO_3 nanorods-rutile TiO_2 nanoparticles core-shell interface for efficient DSSCs, *Dalton Trans.* 42 (2013) 10085-10088.
- [46] S.G. Krishnan, M. Harilal, A. Yar, B.L. Vijayan, J.O. Dennis, M.M. Yusoff, R. Jose, Critical influence of reduced graphene oxide mediated binding of M ($M = \text{Mg}, \text{Mn}$) with Co ions, chemical stability and charge storability enhancements of spinal-type hierarchical MCo_2O_4 nanostructures, *Electrochim. Acta*, 243 (2017) 119-128.
- [47] B. Vidhyadharan, N.K.M. Zain, I.I. Misnon, R.A. Aziz, J. Ismail, M.M. Yusoff, R. Jose, High performance supercapacitor electrodes from electrospun nickel oxide nanowires, *J. Alloy Compd.*, 610 (2014) 143-150.
- [48] K.K. Upadhyay, M. Altomare, S. Eugénio, P. Schmuki, T.M. Silva, M.F. Montemor, On the supercapacitive behaviour of anodic porous WO_3 -based negative electrodes, *Electrochim. Acta*, 232 (2017) 192-201.
- [49] R.-T. Wen, C.G. Granqvist, G.A. Niklasson, Eliminating degradation and uncovering ion-trapping dynamics in electrochromic WO_3 thin films, *Nat. Mater.*, 14 (2015) 996-1001.

[50] I. Aldama, V. Barranco, T. Centeno, J. Ibañez, J. Rojo, Composite electrodes made from carbon cloth as supercapacitor material and manganese and cobalt oxide as battery one, *J. Electrochem. Soc.*, 163 (2016) A758-A765.

[51] B.E. Conway, *Electrochemical supercapacitors: scientific fundamentals and technological applications*, 2nd ed., Kluwer Academic/Plenum Publishers, New York, 1997.

[52] S. Zhang, N. Pan, Supercapacitors performance evaluation, *Adv. Energy Mater.*, 5 (2015) 1401401.

Figure Captions

Scheme 1: Schematic presentation of nanocomposite materials preparation.

Fig. 1. XRD patterns of (a-b) TiO₂, 2 wt% W-TiO₂, 3 wt% W-TiO₂, 5 wt% W-TiO₂, WO₃, and WO₃/TiO₂ nanocomposite.

Fig. 2. FE-SEM images of (a) TiO₂ (b) 2 wt% W-TiO₂ (c) 3 wt% W-TiO₂ (d) 5 wt% W-TiO₂ (e) WO₃ (f) WO₃/TiO₂ nanocomposite.

Fig. 3. Raman spectra of (a) TiO₂, 2, 3 and 5 wt% W-TiO₂ (b) TiO₂, WO₃ and WO₃/TiO₂ nanocomposite (*inset*).

Fig. 4. (a) Comparison of GCD curves of all the electrodes at 1 A·g⁻¹ (b) variation of Q with current density of all the electrodes.

Fig. 5. Comparison of stability of all the electrodes at a current density of 5 A g⁻¹.

Fig. 6. (a) Comparison of CV curves of all the electrodes (b) Variation of Q of all the electrodes with scan rates.

Fig. 7. Comparison of Nyquist plot of all the electrodes; inset is the Nyquist plot at higher frequencies.

Fig. S1. Nitrogen adsorption-desorption isotherms: (a) TiO₂ (b) 2, 3 and 5 wt% W-TiO₂ (c) WO₃ and (d) WO₃/TiO₂ nanocomposites.

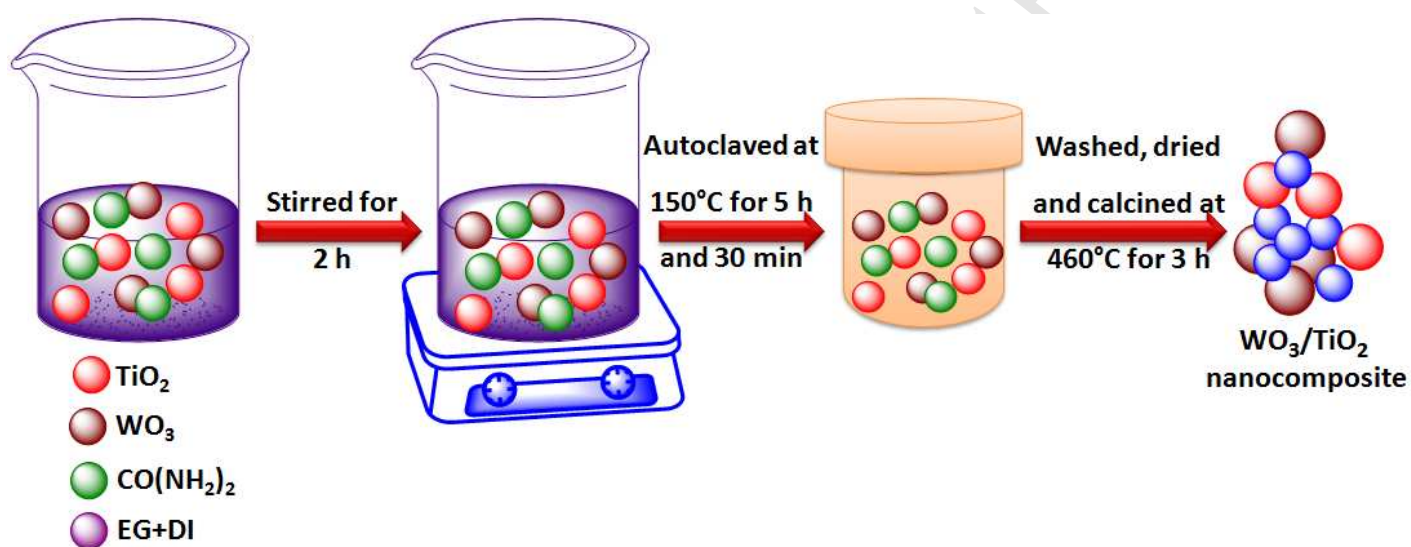
Fig. S2: FT-IR spectra of TiO₂, 2 wt% W-TiO₂, 3 wt% W-TiO₂, 5 wt% W-TiO₂, WO₃ and WO₃/TiO₂ nanocomposites.

Fig. S3. CV of (a) TiO₂ (b) 2 wt% W-TiO₂ (c) 3 wt% W-TiO₂ (d) 5 wt% W-TiO₂ and (e) WO₃ and (f) WO₃/TiO₂ composite electrodes in 6 M KOH aqueous electrolyte with respect to Ag/AgCl reference electrode.

Fig. S4. CDC graph of (a) TiO₂ (b) 2 wt% W-TiO₂ (c) 3 wt% W-TiO₂ (d) 5 at% W-TiO₂ (e) WO₃ and (f) TiO₂/WO₃ nanocomposite.

Fig. S5. (a) CV, (b) CDC and (c) EIS of physically mixed WO₃/TiO₂ (with same ratio) particles.

Figures



Scheme 1: Schematic presentation of nanocomposite materials preparation.

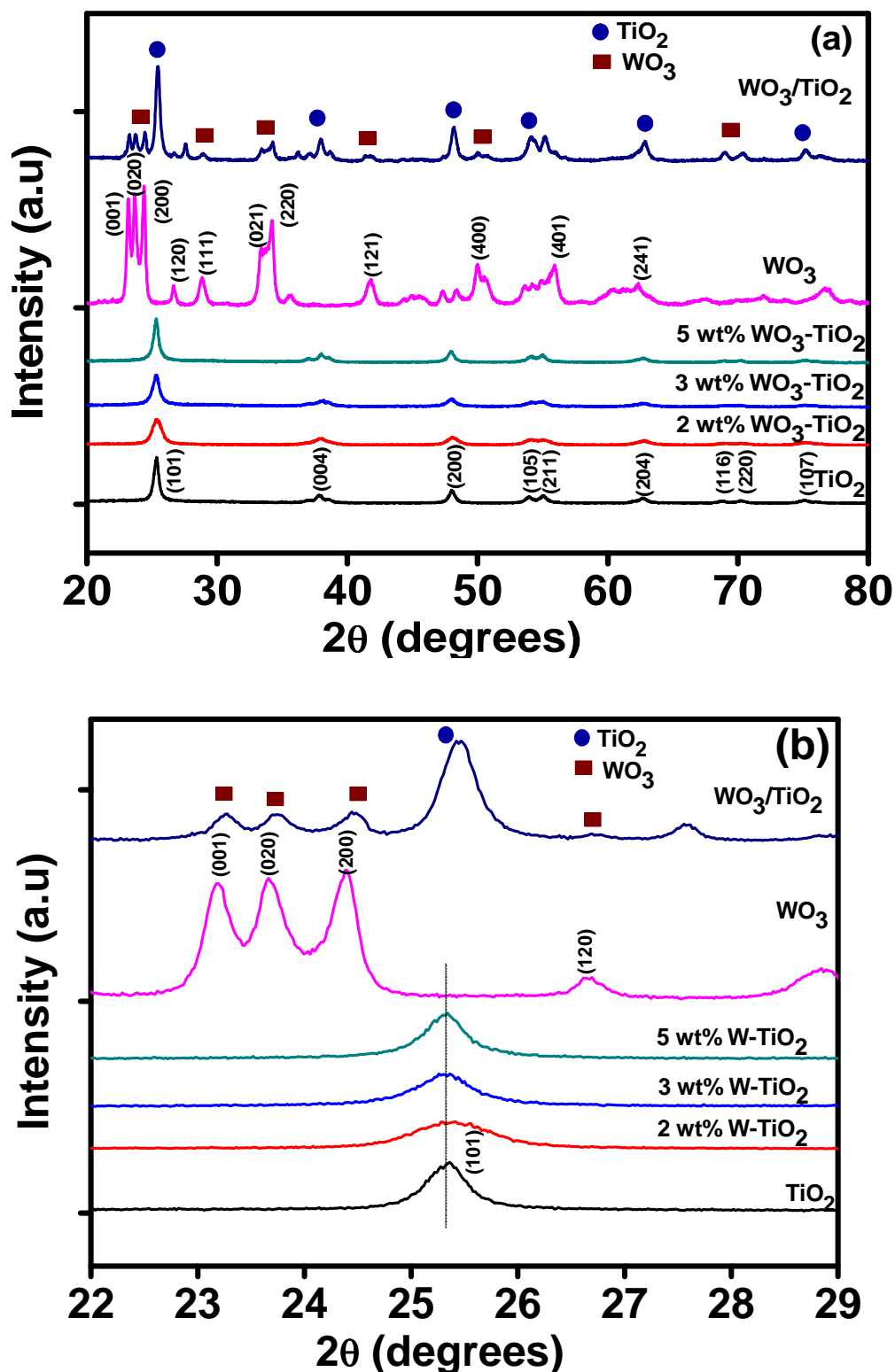


Fig. 1. XRD patterns of (a-b) TiO₂, 2 wt% W-TiO₂, 3 wt% W-TiO₂, 5 wt% W-TiO₂, WO₃, and WO₃/TiO₂ nanocomposite.

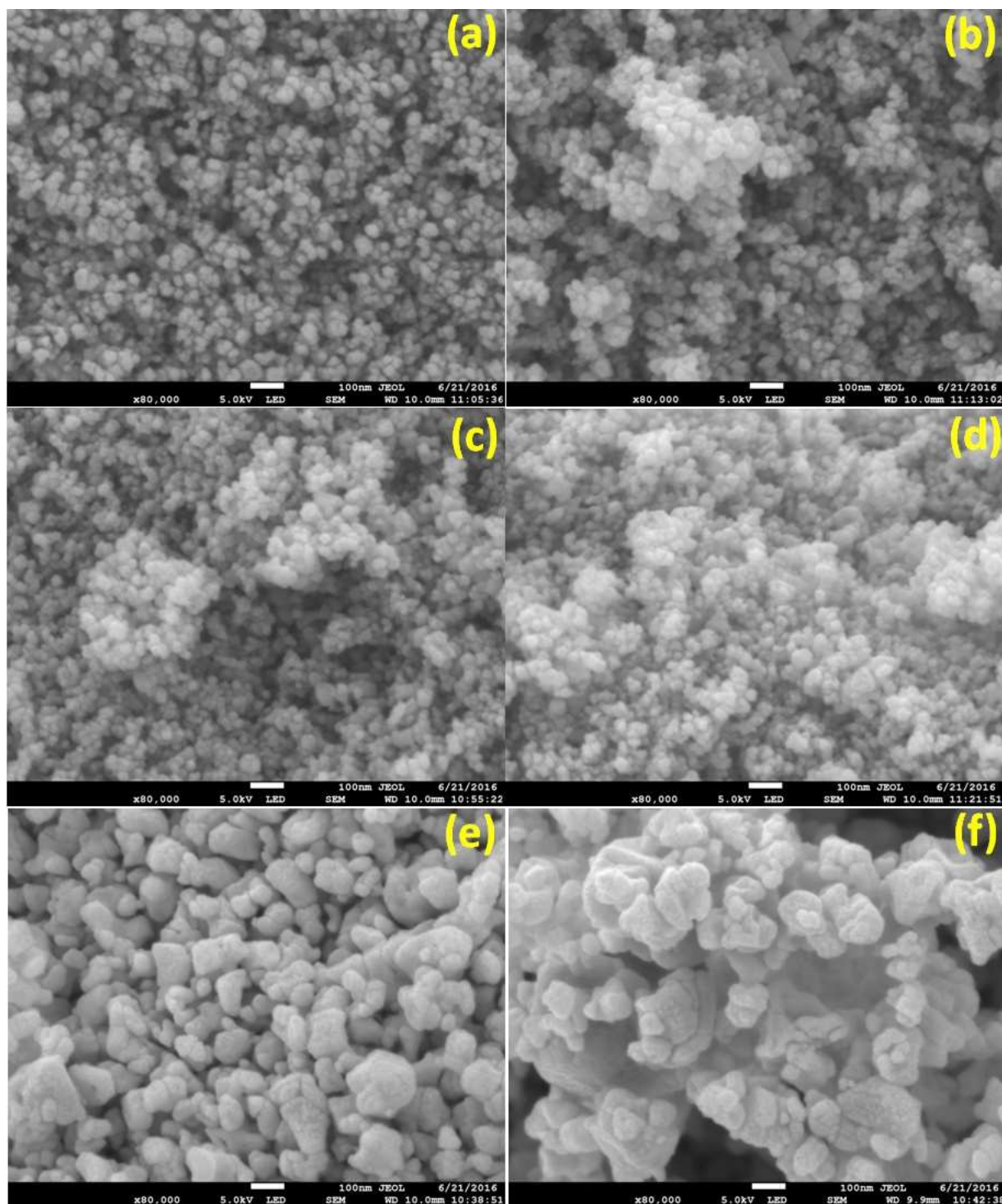


Fig. 2. FE-SEM images of (a) TiO_2 (b) 2 wt% W- TiO_2 (c) 3 wt% W- TiO_2 (d) 5 wt% W- TiO_2 (e) WO_3 (f) WO_3/TiO_2 nanocomposite.

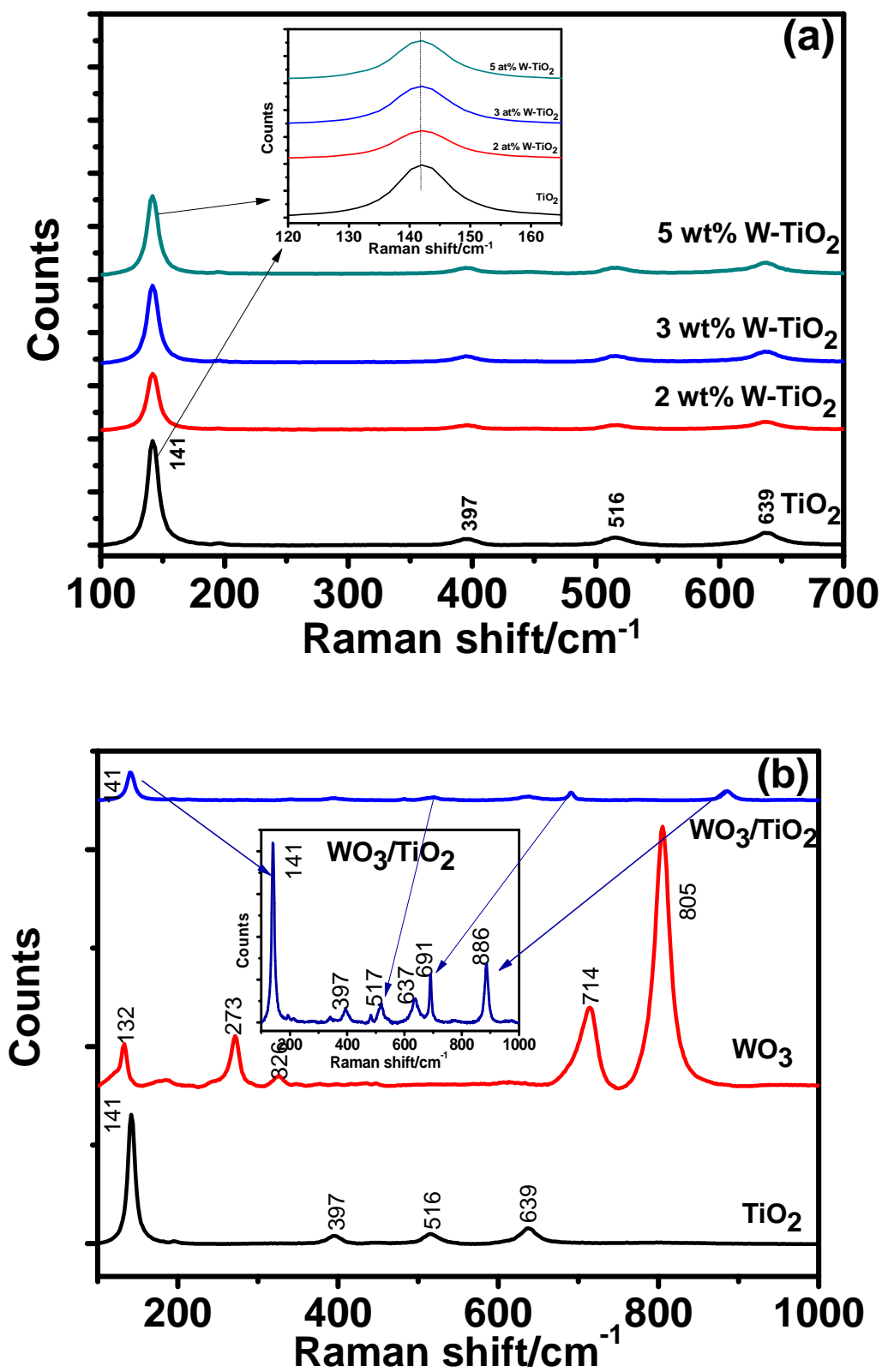


Fig. 3. Raman spectra of (a) TiO₂, 2, 3 and 5 wt% W-TiO₂ (b) TiO₂, WO₃ and WO₃/TiO₂ nanocomposite (*inset*).

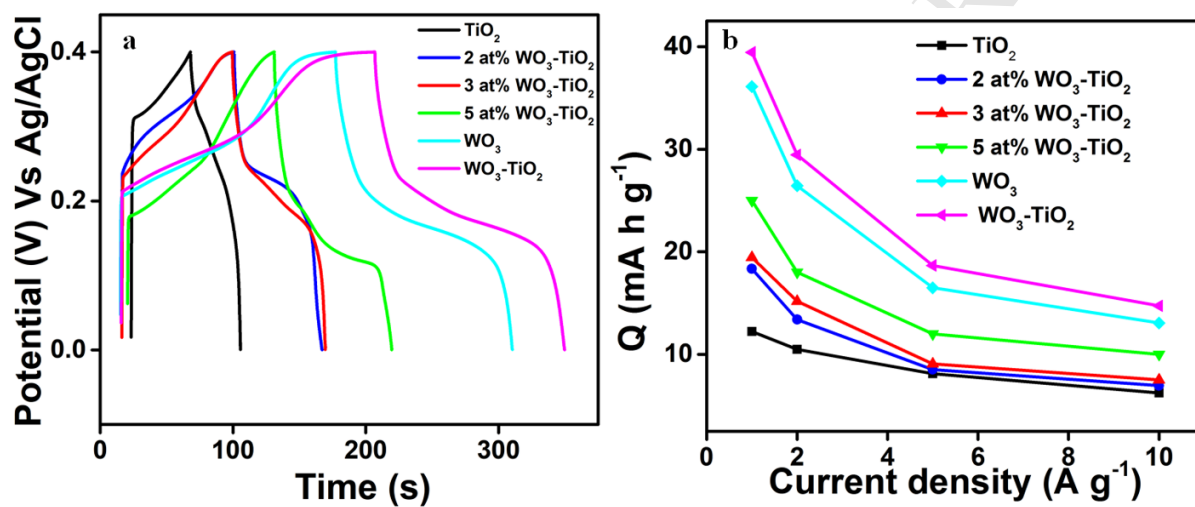


Fig. 4. (a) Comparison of GCD curves of all the electrodes at $1 \text{ A}\cdot\text{g}^{-1}$ (b) variation of Q with current density of all the electrodes.

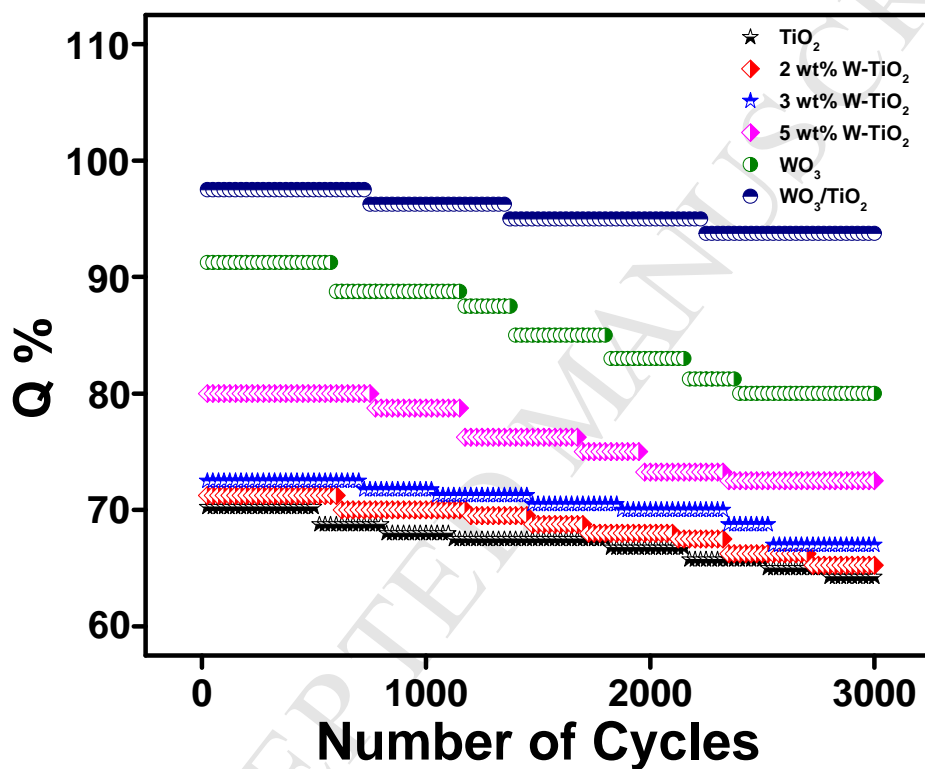


Fig. 5. Comparison of stability of all the electrodes at a current density of 5 A g⁻¹.

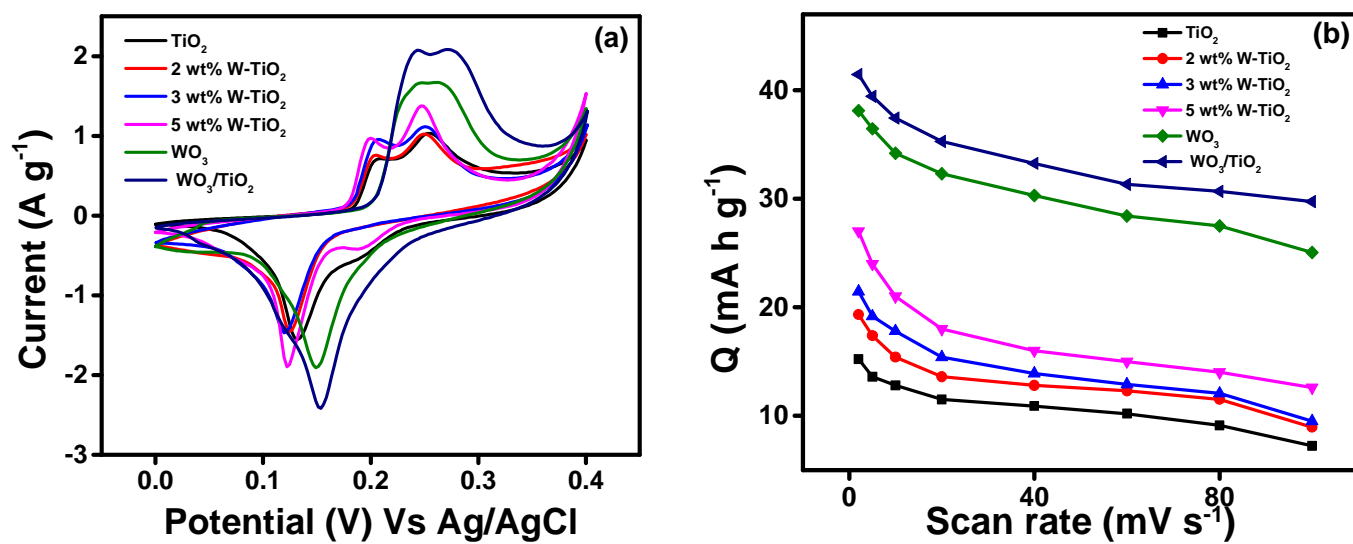


Fig. 6. (a) Comparison of CV curves of all the electrodes (b) Variation of Q of all the electrodes with scan rates.

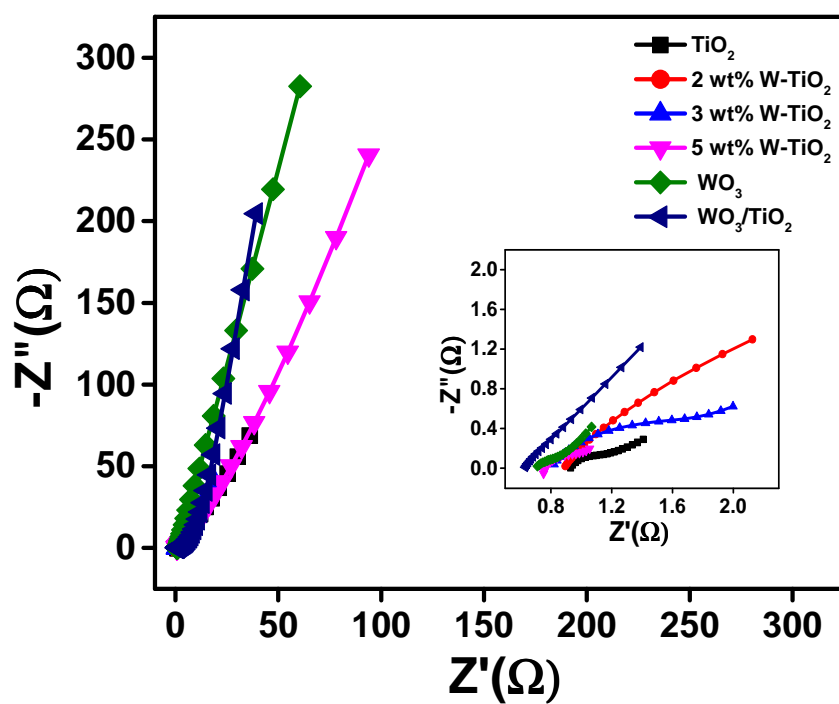


Fig. 7. Comparison of Nyquist plot of all the electrodes; inset is the Nyquist plot at higher frequencies.

Table 1. Lattice Parameters of TiO₂ and 2, 3 and 5 wt% W-TiO₂.

Materials	Lattice parameters (Å)	
	a	c
TiO ₂	3.767	9.699
2 at% W-TiO ₂	3.766	9.698
3 at% W-TiO ₂	3.763	9.695
5 at% W-TiO ₂	3.761	9.693

Research Highlights

- Hydrothermal synthesis of ultrafine metal oxides and composites using oxide precursors.
- This method works well for transition metal doped metal oxide nanostructures.
- The WO_3/TiO_2 composite showed superior charge storability than the single components.
- The above electrode showed superior electrical conductivity and higher ion diffusivity.